RESEARCH PAPER

Super Hydrophilic Nanoporous AC/WS$_2$ QDs/SSM for Highly Efficient Oil-Water Mixture Separation

Elham Garoosi [1], Moayad Hossaini Sadr [2], Alimorad Rashidi [3] *, and Mohammad Yousefi [4]

[1] *Department of Chemistry, Science and Research Branch, Islamic Azad University, Tehran, Iran*

[2] *Department of Chemistry, Faculty of Science, Azarbaijan Shahid Madani University, Tabriz, Iran*

[3] *Nanotechnology Research Center, Research Institute of Petroleum Industry (RIPI), Tehran, Iran*

[4] *Department of Chemistry, Yadegar-e-Imam Khomeini (RAH) Shahr-e-Rey Branch, Islamic Azadmehr University, Tehran, Iran*

ARTICLE INFO

ABSTRACT

The achievement of high-efficiency water/oil separation has significant meaning for maintaining environment and diminishing economic losses; however, there is some challenge at the same time. In this study, the oil-water mixture was separated with simple and low-cost quantum dots metal for the first time by using one-step Nano porous activated carbon (AC)/ Tungsten disulfide (WS$_2$) quantum dots (QDs) stainless still mesh (SSM) as a super hydrophilic and petroleum-based substrate. Nano porous AC/ WS$_2$ QDs was synthesized and characterized by various XRD, FTIR, SEM/ Map, TEM, BET-BJH, PL and CA techniques. The results showed that the solvent type is also effective in the amount of its separation from oil. The effect of water-to-solvent ratio and pH was investigated. Based on the results of petrol with a water-to-solvent ratio of 40/20 at pH=7 and at a time of 14 seconds, 99.99% was separated by Nano porous AC/WS$_2$ QDs/SSM with flux over 6000 $L\,m^{-2}\,h^{-1}$. In order to investigate the effect of solvent of different water and solvent ratios, volumetric ratios of 20/20, 20/40 and 40/20 were examined as a mixture at pH=7. The results showed that the AC/WS$_2$ QDs/SSM of the repeatability cycle is 25 times and its duration to 30 seconds. The results of kinetic studies showed that the pseudo second order kinetic model was in good agreement with the experimental data.

INTRODUCTION

Effluents containing oil-water mixture are produced in many industries such as metalworking, oil refining, petrochemical industries, food industries, leather industries and metal polishing. The sources of these effluents include cooling fluids in metalworking processes, namely metal rolling, metal cutting and wire making, washing baths for cleaning metal parts and car wash effluents [1-3]. A filter surface that has two properties, i.e. hydrophilic and super lipophilic, is suitable for separating water and oil. Such a filter can be produced by the accumulation of activated carbon on metal mesh [4,5]. Separation methods

---

* *Corresponding Author Email: Rashidiam@ripi.ir*

of oil-water mixture include adsorption and Nano filter methods that both use porous substrate, but due to low efficiency, low adsorption rate and secondary pollution, nanomaterials can be used to improve their performance. In meantime, carbon and activated carbon (AC) filters are a good option. AC is a unique material due to its high surface area, high porosity, high adsorption capacity, surface reactivation capability, and low cost. Its important applications are in purification, recycling and separation [6,7]. Carbon materials also have the property of being friendly; therefore, AC has a high lipophilic property owing to its capillary properties. Research has also shown that decreasing surface roughness prevents water leakage. Ergo, the manufacture of metal mesh in which AC is used, can be used to separate oil from water. Metal mesh has high mechanical strength, mass production and high filtration flux [8,9]. Nanomaterials has attracted the attention of many researchers due to their unique physical and chemical properties [10]. Wang et al., prepared flower-like CdS with SDBS surfactant that make the CdS crystals assemble together and also studied its optical properties [11]. Wang et al., fabricated nanostructured CuO films with indium tin oxide - coated glass substrates by electrodeposition method and studied its optical properties [12].

Wang et al., synthesized flower-like ZnO nanostructures assembled by nanosheets and discussion its structural and optical characterization [13]. Yang et al., prepared CdS/TiO2 nanotube and discussed its photocatalytic property [14]. Yang et al., synthesized a series of Zn-doped dendritic-like CdS structures by a simple hydrothermal method that enhanced photocatalytic activity [15]. Wang et al., fabricated diverse CuO nanostructures by a hydrothermal method and investigated their photocatalytic properties [16]. Among these, the QDs are colloidal semiconductor nanocrystals that have high quantum efficiency, wide absorption spectrum, narrow emission with adjustable capability and color stability. The energy gap of these materials depends on several factors, including the type of bond, the bond strength, and the particle size. The phenomenon of quantum constraints causes a wide range of features in these nanoparticles [17]. QDs have different absorption and diffusion properties depending on their size. Among these nanomaterials are families of chemical compounds that are known as dichalcogens intermediate

metals and having shown interesting properties [18-19]. Super hydrophilic materials have also significantly contributed to progress in surface science. The recent extensive research of super hydrophilic coating has been inspired from lotus leaf wetting, known as the "lotus effect" [20-22]. Among these, Nano porous AC/WS₂ is one of the super-hydrophilic materials with the property of separating oil from water. WS₂ is a semiconductor with indirect band gap. This compound has a hexagonal structure and a spatial group of P6₃/mmc. WS₂ has a layer structure in which each layer of tungsten atoms is covalently bonded to S atoms. S-W-S joints are weaker adjacent layers and are made of van der Waals force. The stacked layers in this structure are such that each layer is located along the axis of accumulation of W atoms with a period of rotation after the S atoms, which causes the layer to deviate completely from the flat state [23-26]. Krasian et al., studied a hybrid of 2D materials (MoS₂ and WS₂) as an effective performance enhancer for poly (lactic acid) fibrous mats in oil adsorption and oil/water separation. According to the results, effective separation of surfactant-stabilized oil/water emulsion was obtained with ~70% flux recovery over separating cycles [27]. Zhou et al., delved into electroplating of non-fluorinated superhydrophobic Ni/WC/WS₂ composite coatings with high abrasive resistance. Hardened by WC and lubricated by WS₂ inclusions, the superhydrophobic coatings showed remarkable abrasive resistance with a bearing capacity ≥10,000 mm abrasion length [28]. Cheng et al., investigated hybrid 2D WS₂/GO nanofiltration membranes for finely molecular sieving. The hydrated hybrid WS₂/GO membrane with 15 wt% GO (GO15WS₂) exhibited high rejection (>90%) for dyes and ions with a hydrated radius above 4.9 Å [29]. In this study, i.e. nanoporous AC/WS₂ QDs superhydrophilic composite, reproducibility and fast time were prepared and coated on the mesh for easier collection with one-step hydrothermal method, then They were studied for separation of oil-water mixture. The effect of pH and solvent of different water and solvent ratios were investigated in separation. It should be noted that the stabilization of AC/WS₂ QDs nanoparticles on metal mesh and its application in separating oil-water mixture could be a research innovation.

Nevertheless, there are still many limitations in the synthesis of such filters which have applied uses on manufacturing scale for either industrial

or very small particles, small enough to separate single step water-oil stratified. Moreover, they have a cost-effective, good collection and easy construction method for this purpose.

In this study, nanoporous AC/WS$_2$ QDs superhydrophilic composite, reproducibility, high selectivity, good flux and fast time were prepared and coated on the mesh for more resistance and easier collection with low cost and one-step hydrothermal method for investigating separation of oil-water mixture. It should be noted that the stabilization of AC/WS$_2$ QDs nanoparticles on metal mesh and its application in separating oil-water mixture is a research innovation.

MATERIALS AND METHODS

The raw walnut shells were collected from Tuyserkan, Hamedan province, Iran and East Azerbaijan mines, Iran respectively. Sodium tungstate 99.99% (CAS Number: 13472-45-2), thiourea 99.99% (CAS Number: 62-56-6), Hydrochloric acid 37% (CAS Number: 7647-01-0), potassium hydroxide 99.99% (CAS Number: 1310-58-3), ethanol 96% (CAS Number: 64-17-5), n-Hexane 99% 99% (CAS Number: 110-54-3), toluene, anhydrous, 99.9% (CAS Number: 108-88-3), ethyl acetate anhydrous 99.8% (CAS Number: 141-78-6), Dimethyl ether ≥99.9% (CAS Number: 115-10-6), Dimethyl carbonate anhydrous, ≥99% (CAS Number: 616-38-6) and 1,2-Dichloroethane anhydrous, 99.8%; CAS Number: 107-06-2, diesel and gasoline were prepared, 0.4 micron stainless steel mesh filter was provided by Iran Steel Company.

Nano porous AC synthesis method

Walnut shell was washed, dried and ground. Then, KOH was added following the ratio of 1 to 3. It was placed in a nitrogen atmosphere at 800 $^\circ$C for 1 h. The resulting powder was then washed with 1 mM hydrochloric acid and dried at 120 $^\circ$C in an oven (Fig. 1).

AC/WS$_2$ QDs/SSM synthesis method

0.88 g of Na$_2$WO$_4$, 1.14 g of thiourea and 0.1 g of Nano porous AC with 30 mL of distilled water
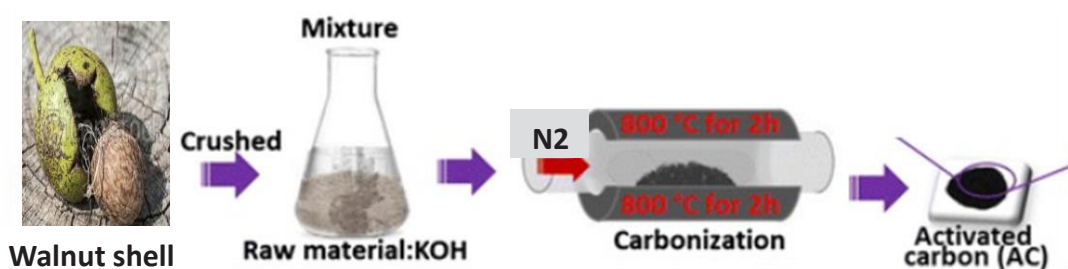

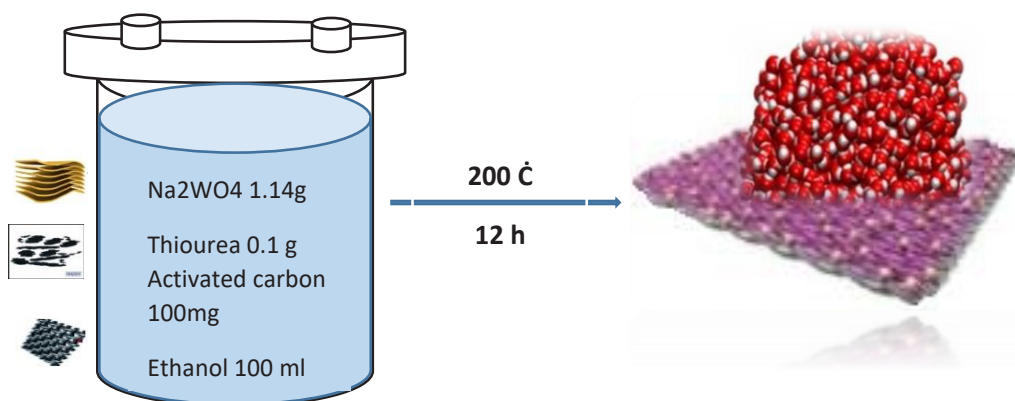Fig. 1. Graphical process for AC synthesis.

Fig. 2. Graphical process for the synthesis of AC/WS$_2$ QDs filter.

and 100 mL of 97% ethanol and metal mesh with a diameter of 5 cm were placed in the autoclave. It was heated for 12 hours at 200 °C in the oven (Fig. 2).

Oil-water mixture separation

First, we put two flange-shaped glass cylinders inside the Teflon and placed the silicone gasket on the bottom cylinder. Then, the mesh, pre-soaked with water, was placed on the washer and the second washer was placed on the mesh; the top cylinder and Teflon were easily wrapped in the lower set to completely seal the two cylinders mesh and washers. Various samples of pure water, petrol, gasoline, hexane, toluene, ethyl acetate, dibutyl ether, dichloroethane, and dimethyl carbonate with volumetric ratios of 20/20, 40/20 20/40 are mixed in pH 5, 7 9 were prepared and the mesh filter was rejected (Fig. 3).

The water contents before and after Nano filter were measured using the Karl Fischer moisture titration method.

The oil absorption capacity was measured by immersing, the Nano porous CA/WS$_2$ QDs/SSM in different oils until saturation.

The kinetic of oil sorption was performed by recording oil sorption at a certain time interval (2 s) by placing AC/WS$_2$ QDs/SSM on the surface of the oil. The time span of the experiment was 2 s to 14 S.

The kinetic of sorption by AC/WS$_2$ QDs/SSM is presented in Table 2. The sorption of all oils increases with sorption time until saturation. The kinetic of oil sorption can be described by pseudo-first, second order and Intra particle diffusion

kinetic model [30]. The equations and values of rate constants are listed in Table 2.

RESULTS AND DISCUSSION

X-ray diffraction analysis

X-ray diffraction (XRD) analysis was used to identify the structure of the material. Fig. 4 shows the scattering pattern of XRD Nano porous AC, WS$_2$ and Nano porous AC/WS$_2$ QDs. In Nano porous AC, the broad (002) diffraction peak (2θ = 15-30º) can be attributed to the amorphous carbon structures. The weak and broad (101) diffraction peak (2θ = 40-50º) is due to the axis of the graphite structure.

In Nano porous AC/WS$_2$ QDs, the peaks at angles 24° and 43° are related to AC and WS$_2$. The diffraction peaks at 2θ value of 15.45°, 29.75°, 30.61° and 51.16° were observed, ascribed to the (002), (004), (100) and (105), the results showed that indexed to the hexagonal WS$_2$ phase with cell constants of a = 3.154 Å and c = 12.362 Å, which is consistent with the standard JCPDS card no. 08-0237.

The crystalline size of the prepared Nano porous AC, WS$_2$ and Nano porous AC/WS$_2$ QDs are calculated using Scherrer's formula:

D signifies crystallite size, λ denotes the cathode wavelength (nm), K is constant equal to 0.89, β FWHM (rad) and θ angle are corresponding to the desired peak.

Table 1 shows the calculated crystalline and lattice parameters of the prepared Nano porous AC, WS$_2$ and Nano porous AC/WS$_2$ QDs.

Proposed Mechanism

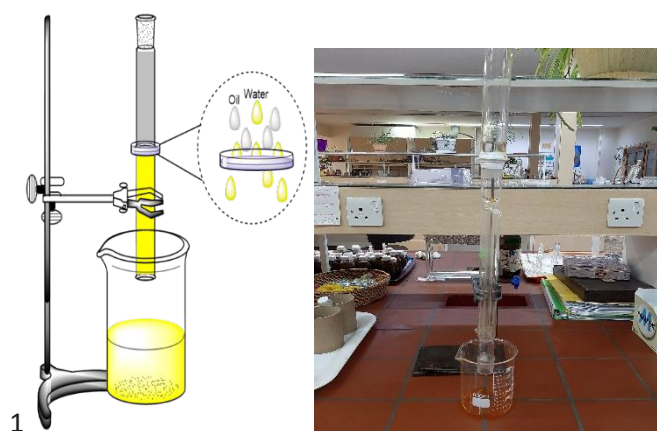Functional groups in the molecular level
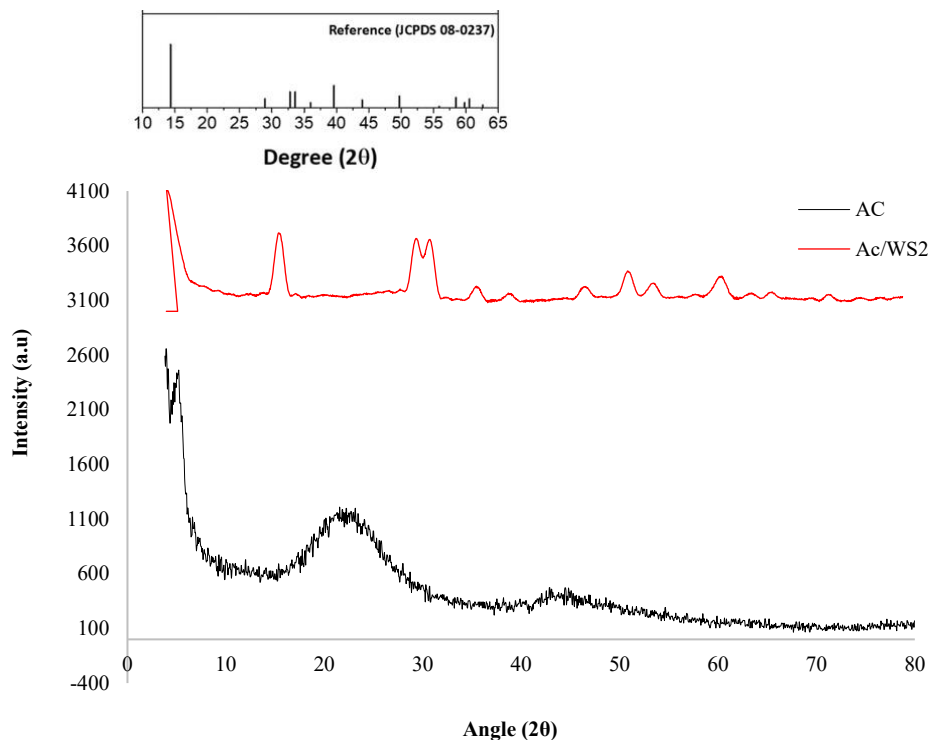

Fig. 3. Separation oil-water mixture separation.

Fig. 4. XRD patterns of the AC and AC/WS$_2$.

Table 1. Lattice parameters of AC, AC/WS$_2$.

Sample	D(nm)
AC	19.80
AC/WS$_2$	18.65

recover the wettability of the surface. Generally, the hydrophilicity is affected by decreasing the carbon length and functional groups shape [31]. Therefore, Ac is a substrate for WS$_2$ QDs, according to the FTIR spectrum advent peak at 700 cm^{-1} and 1100 corresponding to the S-C (Fig. 5). The main pattern is played by WS$_2$ in this matrix. The interaction between the AC/ WS$_2$ QDs surface and hydrocarbon molecules (oil) decreases due to molecular defect of S atoms at the substrate surface (Fig. 13), hence the access of the S atomics to hydrocarbon (oil) molecular decreases and cannot form a bond between sulfur–carbon all of the substrate. This could result in enhancement the interfacial tension, causing the surface to become super hydrophilic.

Fourier-transform infrared spectroscopy

Fig. 5 shows the FTIR spectrum of the prepared Nano porous AC peak at 1095.38 cm^{-1} assigned to C-O-C, at 1628.13 cm^{-1} attributed to C=O and in the peak range of 3442.50 cm^{-1} corresponding to the tensile vibration of OH.

The FT-IR spectra of Nano porous AC/WS$_2$ QDs in the range of 442.53 cm^{-1} for W-S tensile vibration, in the range of 623.79 cm^{-1} for C-S, in the range 10.968 and 1405.29 cm^{-1}, corresponds to C-O-C, in the range 1623.02 cm^{-1} corresponds to C= O, and in the peak range 3427.17 cm^{-1} corresponds to the tensile vibration of OH (Fig. 5).

Photoluminescence analysis

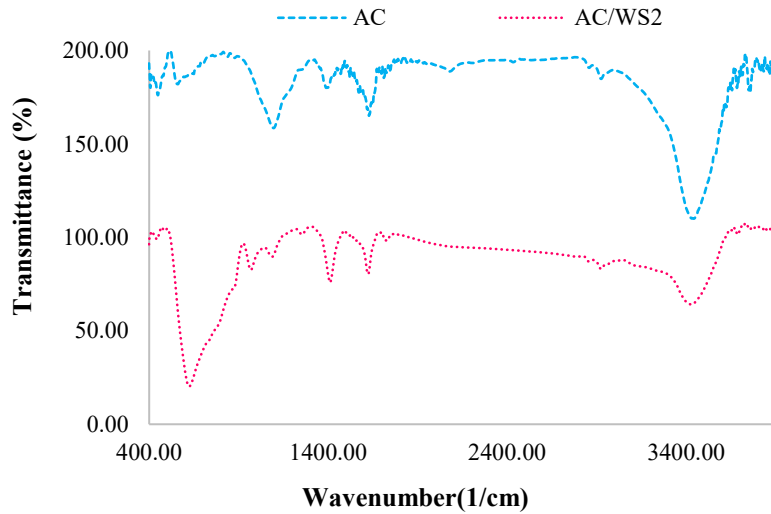During photoluminescence, the solution of WS$_2$

Fig. 5. FTIR patterns of the AC, and AC/WS$_2$.

QDs was obtained by excitation at wavelengths of 300 to 460 nm and in the range of 10 nm. This result is consistent with the spectrum obtained in Fig. 3. The response peaks of the photovoltaic spectrum show a red shift as the wavelength of the action increases. According to this shift, the responses move to higher wavelengths (360 to 420 nm). This indicates a non-uniform distribution of particle size and the effects of quantum constraints. As the stimulus wavelength increases, the intensity of the response increases, reaching its maximum at 340 nm, and then decreases. Therefore, the maximum response intensity in ultraviolet excitation is 340 nm, which is 412 nm blue. The built-in sample has a high intensity. After a few months, the emission spectrum was measured again and the same results were obtained. Therefore, the built-in quantum dots are stable and do not lose their photovoltaic properties (Fig. 6) [32,33].

QDs are nanoparticles with unique light properties that are capable of emitting light of different colors, and the color of the light depends
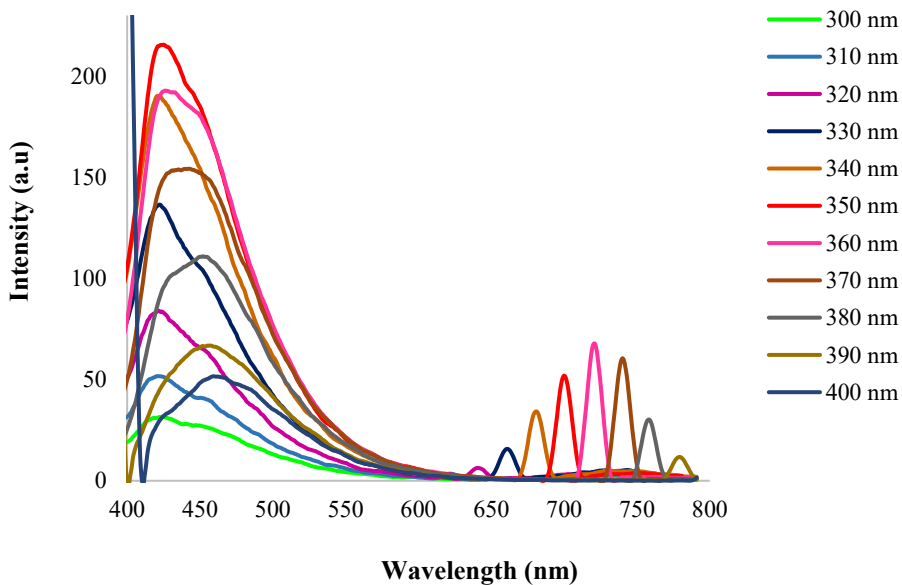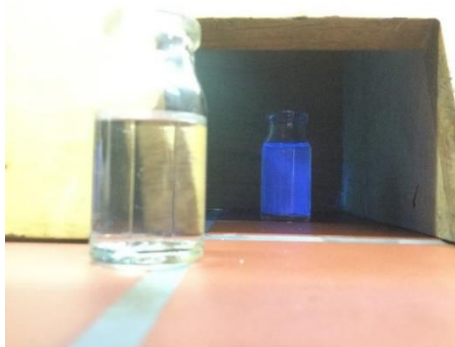

Fig. 6. PL analysis of WS$_2$ QDs.

Fig. 7. Emitting light of WS$_2$ QDs.

on the size of their crystal. In this study, the light emission color of WS$_2$ QDs is blue, indicating that the majority of our QDs sizes are within 2-5 nm range; large blue-shift is expected, as reported in literature (Fig. 7).

SEM analysis

SEM analysis was used to evaluate the morphology and particle size. In the Fig. 8, Nano porous AC, Nano porous AC/WS$_2$ QDs and Nano porous AC/WS$_2$ QDs SSM are respectively shown. The results of WS$_2$ morphology are rod, and Nano porous AC/WS$_2$ particles are well established on the mesh (Fig. 8). Based on the results, the diameter of AC nanoparticles is about 19 nm and the diameter of the rod like WS$_2$ is about 8 nm.

X-ray energy spectroscopy

X-ray energy spectroscopy is an analytical method used to structurally analyze or chemically characterize a sample. In this study, EDS/Map analysis was used to evaluate the weight percentage of AC/WS$_2$ elements. According to the results, the weight percentages of C, S and W were 46.14, 20.89 and 32.43, respectively (Fig. 9).

The Nano porous AC and Nano porous AC/WS$_2$ QDs TEM images are shown in Fig. 10. Nano porous AC TEM image are shown in dimensions of 50 nm. According to the results, the particles are completely uniform and nanoscale. Based on Fig. 10 (b), it can be observed that these Nano Rod are assembled, which are about 100 nm in length and 10 nm in Diameter, respectively. According to the result of TEM, the particle size and morphology of Nano porous AC and Nano porous AC/WS$_2$ QDs are in agreement with the result of XRD and SEM.

BET-BJH Analysis

The measurement of specific surface area, diameter, volume and size distribution of material cavities have very important applications. These methods include absorption-based, diffraction-based, and imaging-based methods. Among these methods, the BET method was introduced in 1938,
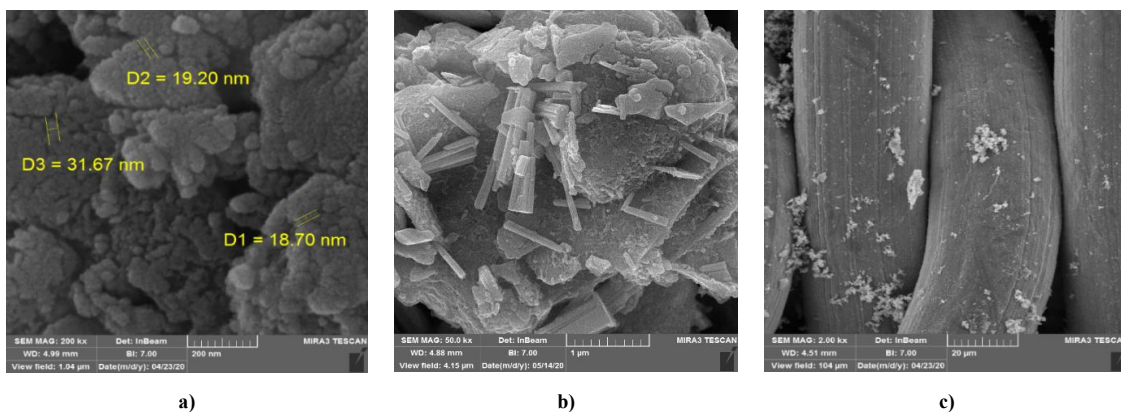

Fig. 8. SEM images of a) AC, b) AC/WS$_2$ and c) AC/WS$_2$ SSM.
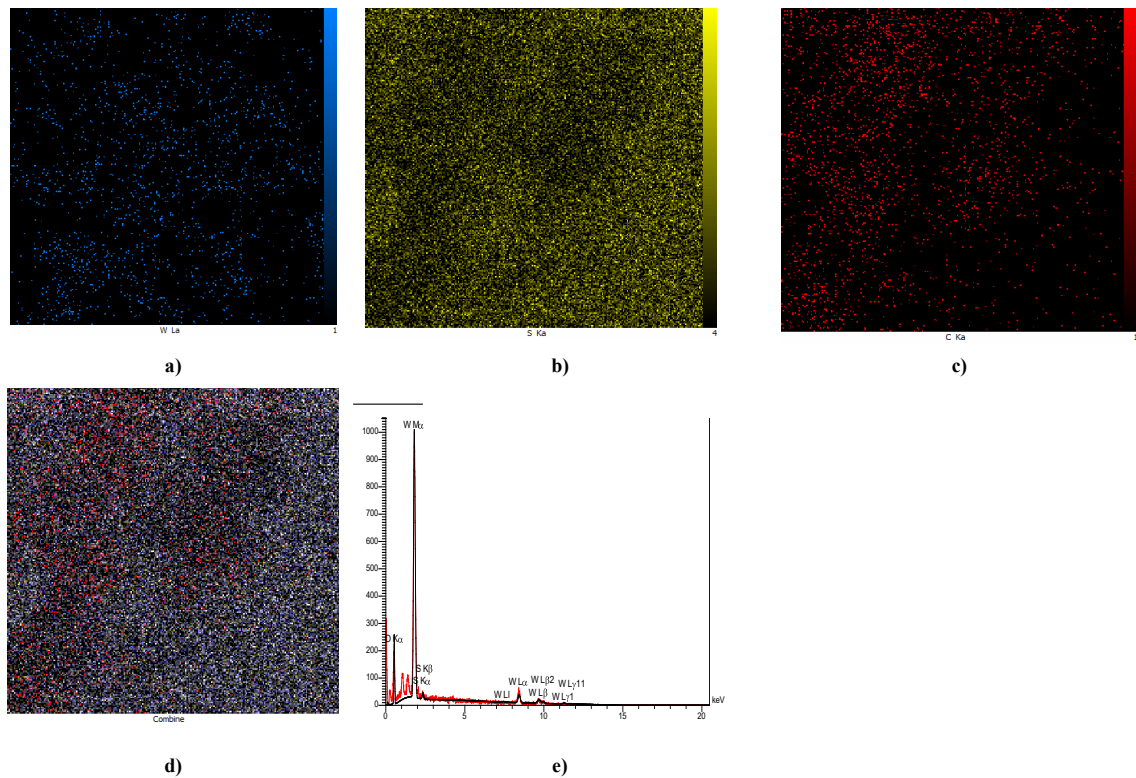
a) b) c)

d) e)

Fig. 9. Map images of a) W, b) S, c) C, d) combine and e) EDS pattern of AC/WS$_2$.

based on absorption, which is much simpler, more accurate and more reliable than other methods. The basis of this method is based on measuring the amount of nitrogen gas absorbed and absorbed by the surface of the material under consideration and at a liquid nitrogen temperature of 77 k. In this way, the cell containing the sample to be analyzed is placed in a liquid nitrogen tank, then
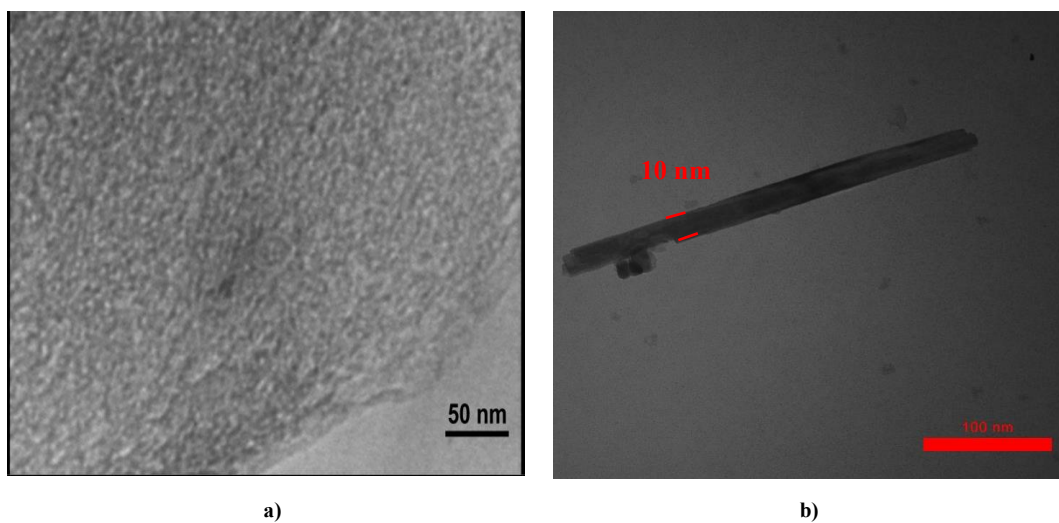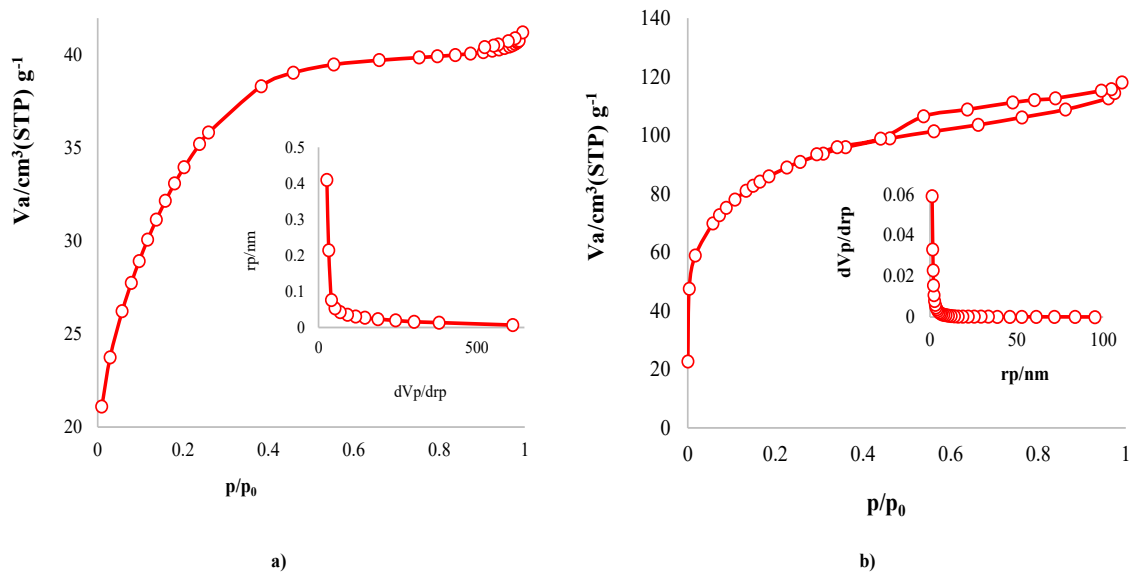

a) b)

Fig. 10. TEM images of a) AC and b) AC/WS$_2$.

Fig. 11. N$_2$ adsorption-desorption isotherms of the a) AC and b) AC/WS$_2$ QDs.

with a gradual increase in nitrogen gas pressure with a high purity percentage during different stages, the amount of gas volume absorption by the material is calculated. The results showed that Nano porous AC and Nano porous AC/WS$_2$ QDs have surface area of 2736.36 and 301.76 (m^2/g), the total volume of cavities are 1.43 and 0.182 cm^3/g , and the average cavities are 20.64 A^0 and 2.41 nm (Fig. 11).

Contact angle analysis

Using the contact angle measurement system, the amount of hydrophilicity and hydrophobicity, can be investigated.

To examine the hydrophilicity property of Nano porous AC/WS$_2$ QDs, contact angle analysis was performed. As seen in Fig. 10, the contact angle of the Nano porous AC/WS$_2$ QDs is under 90 °; therefore, the AC/WS$_2$ QDs is hydrophil. The sample AC/WS$_2$ QDs/SSM with distinguished wettability towards water and oil could be reckoned as a good separation membrane for oil-water mixture separation.

Number of Atomic Vacancy

The cyclic voltametric (CV) diagram (Fig. 13) shows that flow of the curve of AC/MoS$_2$ QDs is very low by 0.8 µA, indicating that there is no

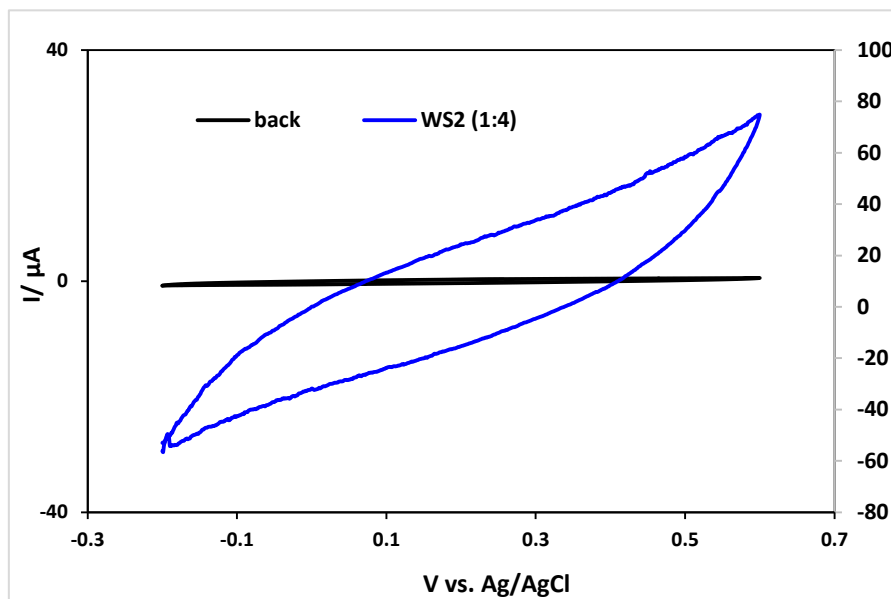Fig. 12. Contact angle of AC/WS$_2$ QDs/SSM.

Fig. 13. CV spectrum for structural defect of AC/MoS$_2$ QDs powder.

structural defect in the molybdenum-sulfide composition due to the approximate molar ratio of 1:2 molybdenum to sulfide. Molybdenum atoms are all covalently bonded to sulfide atoms, and all sulfur atoms interact with hydrocarbons, blocking the passage of water and making the substrate super hydrophilic super oleophobic.

Thickness of layers

AFM analysis was carried out to deals with the effect of Nano porous AC/WS$_2$ QDs and AC/WS$_2$ QDs/SSM on the surface roughness. Fig. 14 indicates the AFM micrographs and the surface topography of the AC/WS$_2$ QDs coated-mesh. AFM results reveal that the Root Mean Square (RMS) roughness (Rq) are 6 µm and 7 µm for AC/WS$_2$ QDs and AC/WS$_2$ QDs/SSM, respectively. Therefore, the surface roughness of AC/WS$_2$ QDs/SSM is higher than of AC/WS$_2$ QDs. Decreasing the surface roughness has led to the conversion of the surface from hydrophilic AC/WS$_2$ to superhydrophilic AC/WS$_2$ QDs/SSM. Furthermore, the micrographs confirm the micro/nanoscale roughness that is the consequence of packing uniform particles of the coating together tightly.
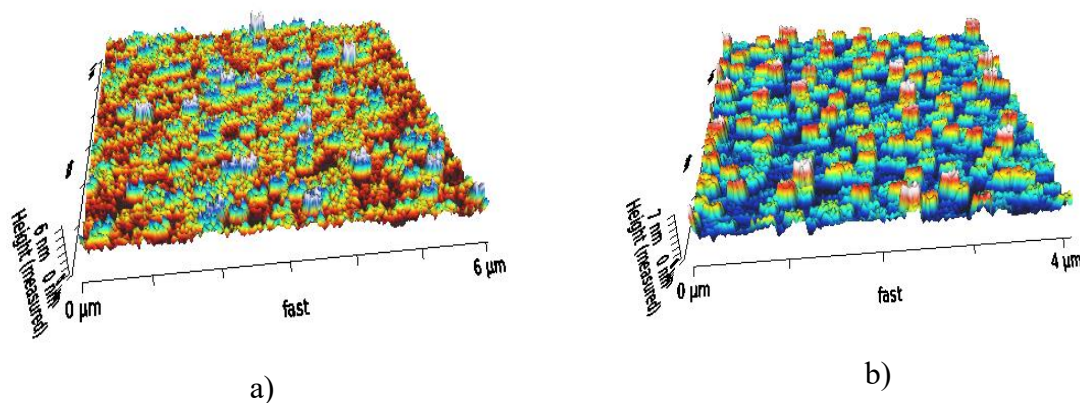
As the AFM analysis shows, the thickness of

a)

b)

Fig. 14. AFM image of AC/WS$_2$ QDs and AC/WS2 QDs/SSM.

the tungsten composite layer is about 6 nm, and according to the Young- Dupre equation [34], which is used to calculate the water contact angle, following as the layer thickness decreases, the contact angle decreases likewise and the surface becomes super hydrophilic.

The contact angle of water is calculated according to the Young-Dupre equation:

$$COS\theta w = [\frac{W(h)}{w\gamma} - 1] \qquad (1)$$

Where wθ denotes the contact angle of water, and wγ is the surface tension of water and W (h) is the solid-liquid interfacial energy obtained from the following relation:

$$W(h) = [\frac{C}{h^8+d} - \frac{A}{12\pi h^2}] \qquad (2)$$

C is the repulsion between liquid and solid, h is the separation fraction, A is the Hammaker constant, and d is the thickness of the AC/WS₂ QDs. As the thickness of the WS₂ layer d decreases, the energy between the solid-liquid surface W (h) increases; as a result, the water contact angle decreases and the surface becomes hydrophilic.

Effect of solvent type, water and solvent ratio on separation efficiency

The amount of water in the oil-water mixture is one of the most effective parameters for the emulsification and stability of the emulsion. As the amount of water increases, so does the amount of unstable coarse emulsion, and as a result of separation, there is an increase. Also, the level of bipolar attraction is highly dependent on the size of the droplets and the distance between the droplets; therefore, in an emulsion that is the same size as the droplets, the distance between the proportional droplets and the inverse of the volume fraction is dispersed. Observing the results obtained from the experiments of the first stage, we conclude that the solvent type is also effective in the amount of its separation from water, because if we compare the results of the separation in pH = 7 (according to the solvent type) to the one used, it can be seen that the heavier the molecular weight of the solvent, the lower the separation value. The effect of petrol, gasoline, hexane, toluene, ethyl acetate, dibutyl ether, dichloroethane (dichloromethane), and dimethyl carbonate was investigated. Based on the results of petrol with a water-to-solvent ratio

of 20/20 at pH = 7 at a time of 14 seconds, 99.99% was separated by AC/WS₂ mesh. Also, in order to investigate the effect of solvent of different water and solvent ratios, volumetric ratios of 20/20, 40/20 and 20/40 were examined as a mixture at pH = 7. The results showed that by increasing the solvent value, the separation efficiency decreased, while by increasing the amount of water, no effect was observed on the separation efficiency (Fig. 15 a) petrol, b) gasoline, c) hexane, d) toluene, e) ethyl acetate, f) dibutyl ether, g) dichloroethane, and h) dimethyl carbonate).

pH effect

One of the effective parameters in the stability and instability of oil-water mixture is pH. At very high and low pH values, emulsions tend to be more stable, while moderate pH values cause emulsion instability. The optimal pH value in the purification of oil-water mixture in gasoline is about 7. In fact, mixtures are more stable at a very high or low pH values (Fig. 16).

Recycling ability

Various samples of pure water, petrol, gasoline and toluene with volumetric ratios of 40/20 were prepared by mixing the pH 7 at 25 °C and the mesh filter was rejected. The results showed that the repeatability cycle for AC / WS₂ porous QDs / SSM with 99.99% efficiency and over 6000 L m⁻² h⁻¹ flux is cycle 25 and its duration is up to 30 seconds.

The experimental data were fitted using kinetic equations [35]. Logergren has defined a pseudo first-order rate equation in the following form:

$$\ln(q_e - q_t) = \ln q_e - k_1 t \qquad (3)$$

Where q_e and q_t (mol.g⁻¹) are the amount of adsorbed material at equilibrium and time t, respectively, and k_1 (min⁻¹) is the rate constant of pseudo first-order adsorption.

The Elovich equation is another rate equation based on adsorbent capacity. In this equation, by using the boundary conditions $q_t = 0$ at t = 0 and $q_t = q_t$ at t = t, we can obtain the following equation:

$$q_t = \frac{1}{\beta}\ln(\alpha\beta) + \frac{1}{\beta}\ln(t) \qquad (4)$$

Where α denotes the initial adsorption rate constant (mol.g⁻¹ min⁻¹) and signifies β desorption rate constant (g. mol⁻¹) during the experiment. The Elovich equation is commonly used to determine
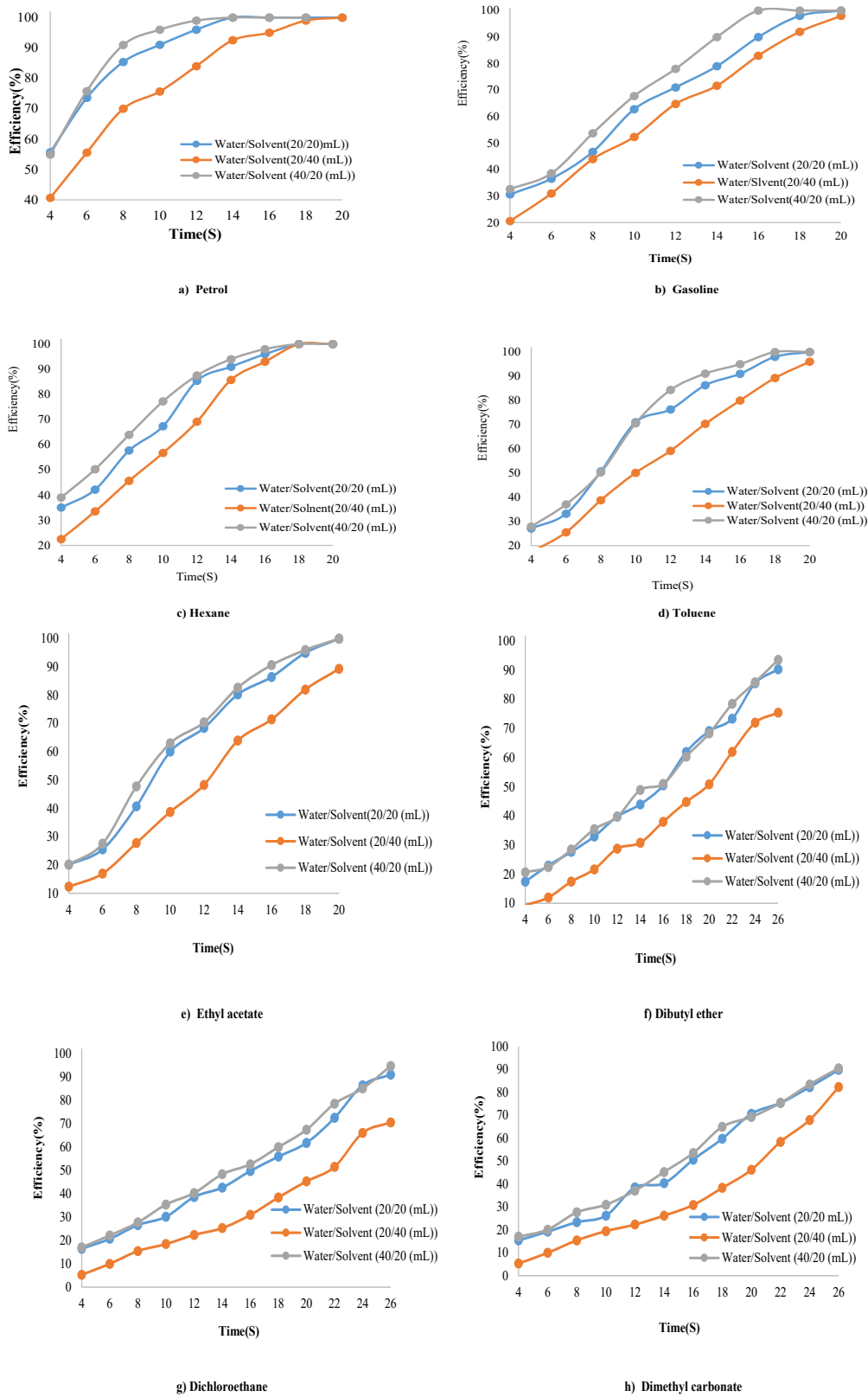
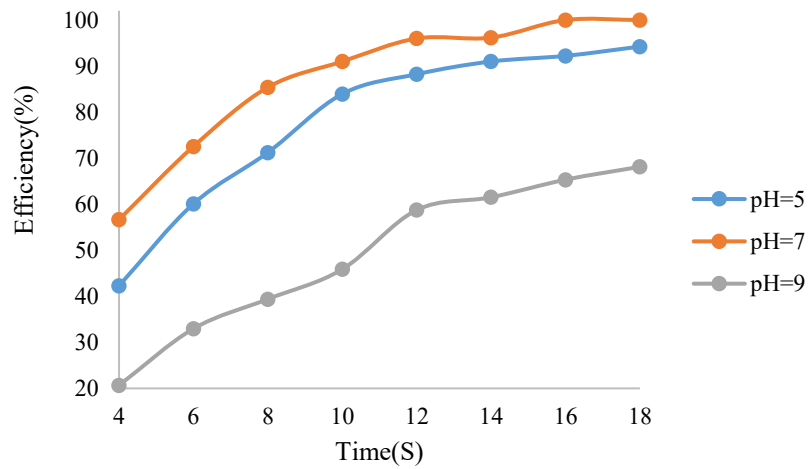Fig. 15. Effect of solvent type and water and solvent ratio.

Fig. 16. The effect of pH.

Table 2. Results of kinetic models.

Kinetic model	General Formula			
		k_1	q_e	R^2
Pseudo first order constants	$\ln(q_e - q_t) = \ln q_e - k_1 t$	0.022	35.402	0.9432
		k_2	q_e	R^2
Pseudo second order constants	$\dfrac{t}{q_t} = \dfrac{1}{k_2 q_e^2} + \dfrac{t}{q_e}$	0.0006	52.651	0.9963
		k_i	C	R^2
Intra-particle diffusion control	$q_t = k_i t^{\frac{1}{2}} + C$	0.432	17.193	0.9764

Table 3. Comparison of previous studies with this research in separation oil in water.

	flux	efficiency	Ref
Cotton-based material (SCM) using poly(vinyl phenol), 1,3-phenylene bisoxazoline	867,500 L m^{-2}h^{-1} bar^{-1}	>99.97%	[36]
Self-cleaning titania robust mesh	1695 L m^{-2}h^{-1}	99.2%	[37]
PDA/PEI@CNTs-NH$_2$	3946.3 L m^{-2} h^{-1}	99.5%	[38]
Zwitterionic functionalized MoS2 nanosheets	108.3 L m^{-2} h^{-1}	99%	[39]
MoS$_2$/GO filtration	48.27 Lm^{-2}h^{-1}	99.5%	[40]
AC/WS$_2$ QDs/SSM	> 6000 L m^{-2} h^{-1}	99.99%	This work

the kinetics of liquid adsorption on heterogenous solids.

Blanchard (1984) , for the first time reported a pseudo second-order rate equation for ion exchange reactions. McKay and Ho defined the linear form of the pseudo second-order rate

equation as follows:

$$\frac{t}{q_t} = \frac{1}{k_2 q_e^2} + \frac{1}{q_e} t \tag{5}$$

Where k_2 (g.moL^{-1}.min^{-1}) is the rate constant of pseudo second-order adsorption.

Based on results, Blanchard kinetic model has the highest agreement with experimental data (Table 2).

The experimental data were fitted using kinetic equations. Based on results, Blanchard kinetic model has the highest agreement with experimental data (Table 2) and the results of this research are shown with the research of others in Table 3.

CONCLUSION

In this study, by Nano filter and the use of a mesh as a hydrophilic with contact angle below 90° and petroleum-based substrate, the oil mixture was separated from the water. Observing the results obtained from the experiments of the first stage, we concluded that the with different type of solvents in the different amount of its for separation from water. Based on the results of petrol with a water-to-solvent ratio of 40/20 at pH = 7 and at a time of 14 seconds, 99.99% was separated by Nano porous AC/WS$_2$ QDs/SSM and over 6000 flux L m^{-2} h^{-1}.The results showed that with the Nano porous AC/WS$_2$ QDs/SSM, the repeatability cycle is 25 times and its duration to 30 seconds and Blanchard kinetic model was in good agreement with the experimental data. As shown in this study, the stabilization of AC/WS$_2$ QDs nanoparticles on metal mesh and its application in the separation of oil from water is an efficient and inexpensive materials with high flux, high repeatability and simple method of research innovation which can be used in future studies even on industrial scale.

CONFLICT OF INTEREST

The authors declare that there is no conflict of interests regarding the publication of this manuscript.

REFERENCES

1. Yin Y, Li H, Zhu L, Guo T, Li X, Xing W, et al. A durable mesh decorated with polydopamine/graphene oxide for highly efficient oil/water mixture separation. Appl Surf Sci. 2019;479:351-359.
2. Karki HP, Kafle L, Kim HJ. Modification of 3D polyacrylonitrile composite fiber for potential oil-water mixture separation. Sep Purif Technol. 2019;229:115840.
3. Zhang N, Qi Y, Zhang Y, Luo J, Cui P, Jiang W. A Review on Oil/Water Mixture Separation Material. Industrial & Engineering Chemistry Research. 2020;59(33):14546-14568.
4. Lin J, Lin F, Liu R, Li P, Fang S, Ye W, et al. Scalable fabrication of robust superhydrophobic membranes by one-step spray-coating for gravitational water-in-oil emulsion separation. Sep Purif Technol. 2020;231:115898.
5. Yin X, Wang Z, Shen Y, Mu P, Zhu G, Li J. Facile fabrication of superhydrophobic copper hydroxide coated mesh for effective separation of water-in-oil emulsions. Sep Purif Technol. 2020;230:115856.
6. Saber A, Mortazavian S, James DE, Hasheminejad H. Optimization of Collaborative Photo-Fenton Oxidation and Coagulation for the Treatment of Petroleum Refinery Wastewater with Scrap Iron. Water, Air, & Soil Pollution. 2017;228(8).
7. Zhang D, Jin X-Z, Huang T, Zhang N, Qi X-d, Yang J-h, et al. Electrospun Fibrous Membranes with Dual-Scaled Porous Structure: Super Hydrophobicity, Super Lipophilicity, Excellent Water Adhesion, and Anti-Icing for Highly Efficient Oil Adsorption/Separation. ACS Applied Materials & Interfaces. 2019;11(5):5073-5083.
8. Sharma M, Jain P, Varanasi JL, Lal B, Rodríguez J, Lema JM, et al. Enhanced performance of sulfate reducing bacteria based biocathode using stainless steel mesh on activated carbon fabric electrode. Bioresour Technol. 2013;150:172-180.
9. Jain A, Balasubramanian R, Srinivasan MP. Hydrothermal conversion of biomass waste to activated carbon with high porosity: A review. Chem Eng J. 2016;283:789-805.
10. Deliyanni EA. Low-cost activated carbon from rice wastes in liquid-phase adsorption. Advanced Low-Cost Separation Techniques in Interface Science: Elsevier; 2019. p. 101-123.
11. Wang Y, Yang X, Ma Q, Kong J, Jia H, Wang Z, et al. Preparation of flower-like CdS with SDBS as surfactant by hydrothermal method and its optical properties. Appl Surf Sci. 2015;340:18-24.
12. Wang Y, Jiang T, Meng D, Yang J, Li Y, Ma Q, et al. Fabrication of nanostructured CuO films by electrodeposition and their photocatalytic properties. Appl Surf Sci. 2014;317:414-421.
13. Wang Y, Ma Q, Jia H, Wang Z. One-step solution synthesis and formation mechanism of flower-like ZnO and its structural and optical characterization. Ceram Int. 2016;42(9):10751-10757.
14. Yang X, Wang Y, Wang Z, Lv X, Jia H, Kong J, et al. Preparation of CdS/TiO$_2$ nanotube arrays and the enhanced photocatalytic property. Ceram Int. 2016;42(6):7192-7202.
15. Yang X, Wang Z, Lv X, Wang Y, Jia H. Enhanced photocatalytic activity of Zn-doped dendritic-like CdS structures synthesized by hydrothermal synthesis. J Photochem Photobiol A: Chem. 2016;329:175-181.
16. Wang Y, Wang D, Yan B, Chen Y, Song C. Fabrication of diverse CuO nanostructures via hydrothermal method and their photocatalytic properties. Journal of Materials Science: Materials in Electronics. 2016;27(7):6918-6924.
17. Khosravi M, Azizian S. Preparation of superhydrophobic and superoleophilic nanostructured layer on steel mesh for oil-water separation. Sep Purif Technol. 2017;172:366-373.
18. Huang Y, Zhan H, Li D, Tian H, Chang C. Tunicate cellulose nanocrystals modified commercial filter paper for efficient oil/water separation. J Membr Sci. 2019;591:117362.

19. Garousi E, Hossaini Sadr M, Rashidi A, Yousefi M. MoS$_2$ QDs-nanoparticle-engineered based hydrophobic filter for high performance water-oil separation. Inorg Chem Commun. 2022;138:109223.

20. Gong X, Zhang L, He S, Jiang S, Wang W, Wu Y. Rewritable superhydrophobic coatings fabricated using water-soluble polyvinyl alcohol. Materials & Design. 2020;196:109112.

21. Sharma V, Sharma V, Goyat MS, Hooda A, Pandey JK, Kumar A, et al. Recent progress in nano-oxides and CNTs based corrosion resistant superhydrophobic coatings: A critical review. Prog Org Coat. 2020;140:105512.

22. Gu J, Fan H, Li C, Caro J, Meng H. Robust Superhydrophobic/Superoleophilic Wrinkled Microspherical MOF@rGO Composites for Efficient Oil–Water Separation. Angew Chem. 2019;131(16):5351-5355.

23. Wu C, Wang S, Zhao J, Liu Y, Zheng Y, Luo Y, et al. Biodegradable Fe(III)@WS$_2$-PVP Nanocapsules for Redox Reaction and TME-Enhanced Nanocatalytic, Photothermal, and Chemotherapy. Adv Funct Mater. 2019;29(26):1901722.

24. Cao J, Zhou J, Chen J, Wang W, Zhang Y, Liu X. Effects of Phase Selection on Gas-Sensing Performance of MoS$_2$ and WS$_2$ Substrates. ACS Omega. 2020;5(44):28823-28830.

25. Charge Transport in 2D MoS$_2$, WS$_2$, and MoS$_2$-WS$_2$ Heterojunction-Based Field-Effect Transistors: Role of Ambipolarity. American Chemical Society (ACS).

26. Ghosh S, Brüser V, Kaplan-Ashiri I, Popovitz-Biro R, Peglow S, Martínez JI, et al. Cathodoluminescence in single and multiwall WS$_2$ nanotubes: Evidence for quantum confinement and strain effect. Applied Physics Reviews. 2020;7(4):041401.

27. Krasian T, Punyodom W, Worajittiphon P. A hybrid of 2D materials (MoS$_2$ and WS$_2$) as an effective performance enhancer for poly(lactic acid) fibrous mats in oil adsorption and oil/water separation. Chem Eng J. 2019;369:563-575.

28. Zhou J, Zhao G, Li J, Chen J, Zhang S, Wang J, et al. Electroplating of non-fluorinated superhydrophobic Ni/WC/WS$_2$ composite coatings with high abrasive resistance. Appl Surf Sci. 2019;487:1329-1340.

29. Cheng P, Chen Y, Gu Y-H, Yan X, Lang W-Z. Hybrid 2D WS$_2$/GO nanofiltration membranes for finely molecular sieving. J Membr Sci. 2019;591:117308.

30. Xia H, Wu S, Liu Y. Photoelectrochemically active perovskite QDs/TiO$_2$ inverse opal with enhanced photoluminescence intensity. Nanotechnology. 2020;31(20):205704.

31. Xu Y, Yan L, Li X, Xu H. Fabrication of transition metal dichalcogenides quantum dots based on femtosecond laser ablation. Sci Rep. 2019;9(1).

32. Santalucia R, Vacca T, Cesano F, Martra G, Pellegrino F, Scarano D. Few-Layered MoS$_2$ Nanoparticles Covering Anatase TiO$_2$ Nanosheets: Comparison between Ex Situ and In Situ Synthesis Approaches. Applied Sciences. 2020;11(1):143.

33. Wang T, Hu X, Zhang X, Cao H, Huang Y, Feng P. MoS$_2$ QDs co-catalytic Fenton reaction for highly sensitive photoluminescence sensing of H$_2$O$_2$ and glucose. Analytical Methods. 2019;11(4):415-420.

34. Schrader ME. Young-Dupre Revisited. Langmuir. 1995;11(9):3585-3589.

35. Fard NE, Fazaeli R, Ghiasi R. Band Gap Energies and Photocatalytic Properties of CdS and Ag/CdS Nanoparticles for Azo Dye Degradation. Chemical Engineering & Technology. 2015;39(1):149-157.

36. Daksa Ejeta D, Wang C-F, Kuo S-W, Chen J-K, Tsai H-C, Hung W-S, et al. Preparation of superhydrophobic and superoleophilic cotton-based material for extremely high flux water-in-oil emulsion separation. Chem Eng J. 2020;402:126289.

37. Kang H, Cheng Z, Lai H, Ma H, Liu Y, Mai X, et al. Superlyophobic anti-corrosive and self-cleaning titania robust mesh membrane with enhanced oil/water separation. Sep Purif Technol. 2018;201:193-204.

38. Zuo J, Liu Z, Zhou C, Zhou Y, Wen X, Xu S, et al. A durable superwetting clusters-inlayed mesh with high efficiency and flux for emulsion separation. J Hazard Mater. 2021;403:123620.

39. Liang X, Wang P, Wang J, Zhang Y, Wu W, Liu J, et al. Zwitterionic functionalized MoS$_2$ nanosheets for a novel composite membrane with effective salt/dye separation performance. J Membr Sci. 2019;573:270-279.

40. Ma J, Tang X, He Y, Fan Y, Chen J, HaoYu. Robust stable MoS$_2$/GO filtration membrane for effective removal of dyes and salts from water with enhanced permeability. Desalination. 2020;480:114328.